

REGAS: REspiratory-GAted Synthesis of Views for Multi-Phase CBCT Reconstruction from a single 3D CBCT Acquisition

Cheng Peng¹, Haofu Liao², S. Kevin Zhou^{3,4}, Rama Chellappa¹

¹ Johns Hopkins University, ² University of Rochester

³ School of Biomedical Engineering & Suzhou Institute for Advanced Research Center for Medical Imaging, Robotics, and Analytic Computing & LEarning (MIRACLE), University of Science and Technology of China

⁴ Key Lab of Intelligent Information Processing of Chinese Academy of Sciences (CAS), Institute of Computing Technology cpeng26@jh.edu

Abstract

It is a long-standing challenge to reconstruct Cone Beam Computed Tomography (CBCT) of the lung under respiratory motion. This work takes a step further to address a challenging setting in reconstructing a **multi-phase** 4D lung image from just a **single** 3D CBCT acquisition. To this end, we introduce **RE**spiratory-**G**ated **S**ynthesis of views, or **REGAS**. REGAS proposes a self-supervised method to synthesize the undersampled tomographic views and mitigate aliasing artifacts in reconstructed images. This method allows a much better estimation of between-phase Deformation Vector Fields (DVs), which are used to enhance reconstruction quality from direct observations *without synthesis*. To address the large memory cost of deep neural networks on high-resolution 4D data, REGAS introduces a novel Ray Path Transformation (RPT) that allows for *distributed, differentiable* forward projections. REGAS require no additional measurements like prior scans, air-flow volume, or breathing velocity. Our extensive experiments show that REGAS significantly outperforms comparable methods in quantitative metrics and visual quality.

Introduction

Cone Beam Computed Tomography (CBCT) is a medical imaging technique widely adopted in dentistry, image-guided radiation therapy, etc. CBCT acquires 2D tomographic views of 3D object by emitting radiation from a rotating gantry, as shown in Fig. 1a, and use these views for 3D reconstruction (Feldkamp, Davis, and Kress 1984). Compared to traditional CT, a CBCT scanner emits less radiation on patients (Elstrøm et al. 2011), is less expensive, and is more flexible.

Accurate lung CBCT imaging is of significant clinical value, especially given the Coronavirus pandemic. However, lung CBCT imaging is affected by the *motion-induced* inconsistencies between acquired views and the subsequent motion artifacts in reconstructions, as shown in Fig. 1b. A common way to address this is to model the breathing motion as a cyclical process and approximate it by a number of 3D CBCTs, referred to as *phases*. Under this model, each view is attributed to one of the phases for reconstruction. The phase-view correspondence can be obtained either through dedicated physical devices (Beaudry 2015) or through signal processing on acquisition data (Yan et al. 2013). This is known as respiratory-gated 4D CBCT reconstruction. While

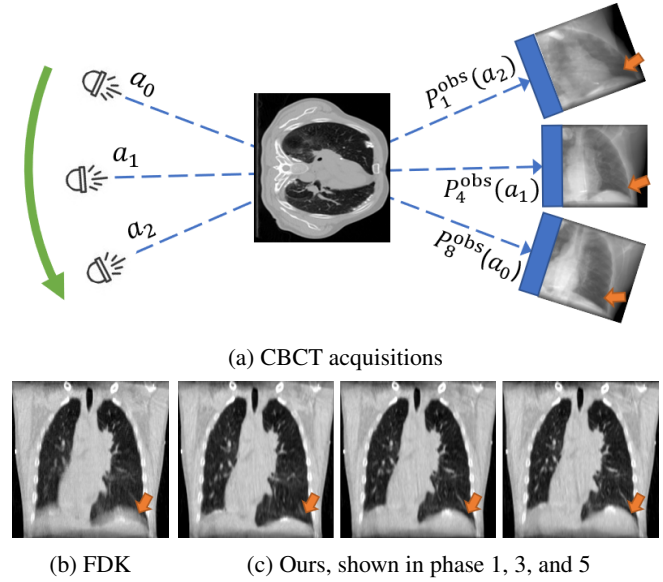


Figure 1: The respiratory motion leads to inconsistencies between projections, thus the traditionally reconstructed image, *e.g.* in 1b, contains significant motion blur. Our proposed REGAS can disentangle the observed motion, as indicated by the orange arrows in 1c.

motion is disentangled by the phase dimension, each phase corresponds to only a portion of the acquired views; therefore, *a high quality 4D CBCT requires a large number of views to faithfully reconstruct each phase*. This leads to a trade-off between a longer scan time and higher radiation dosage, or lower image qualities with few views, similar to a regular 3D CBCT acquisition.

Reconstructing 4D CBCT with limited acquisitions is a difficult problem. Existing methods (i) rely on handcrafted regularizers to address the aliasing artifacts, *e.g.* through spatial or temporal Total Variation (TV) (Andersen and Kak 1984; Blondiaux et al. 2017), or (ii) require additional information like prior scans, air-flow volume and velocity, deformation vector field (DVF) model, etc. (Brock, Docef, and Murphy 2010; Chee et al. 2019; Ren et al. 2012; Wang and Gu 2013), which introduces additional devices and costs into the process. Many deep learning based (DL-based) methods use supervised learning to suppress sparse-view artifacts,

e.g. (Chen et al. 2020; Han and Ye 2018; Zhang, Li, and Chen 2021); however, these end-to-end methods are applicable only to 2D CT due to the heavy computational and data requirements. Furthermore, factors such as scanner differences and breathing motion differences can lead to generalization issues from supervised training.

We propose a novel 4D CBCT reconstruction method called REspiratory-GAted Synthesis of views (**REGAS**), which combines the advantages of traditional methods and DL-based methods. We note that a key component to address 4D CBCT reconstruction is inter-phase deformation modeling; i.e., we can obtain high quality 4D CBCT reconstruction if the breathing DVF is known. However, obtaining such DVF is extremely difficult with limited acquisitions due to noisy reconstruction and a lack of groundtruth. To address the reconstruction, REGAS first synthesizes the unobserved views of each phase through a Convolutional Neural Network (CNN). The synthesized views are then combined with the observed views for reconstruction, which addresses the undersampled condition and the subsequent streaky artifacts. More accurate DVFs are estimated based on our improved reconstructions, and are used to further update individual phases from observed views only.

REGAS has several advantages compared to previous DL-based methods. Firstly, REGAS is **self-supervised**; it synthesizes unobserved views by leveraging the 3D geometric consistency from undersampled phases and the texture similarity to observed views, which is captured by a self-supervised adversarial loss. Furthermore, REGAS is **scalable to high resolution** through our novel Ray Path Transformation (RPT), which allows for distributed, differentiable forward projections. Therefore, REGAS can synthesize views that are **geometrically consistent and of high fidelity**, while requiring no groundtruth for training. The synthesized views lead to higher quality reconstructions, which assist in better DVF estimation. The accurate DVF estimation enables us to obtain synthesis-free reconstructions and eliminate concerns about the reliability of generative methods.

Our contributions can be summarized in four parts:

1. We propose REGAS, which formulates respiratory-gated 4D CBCT reconstruction as a view completion problem. REGAS incorporates the physical imaging geometry with a combination of 3D and 2D CNNs.
2. We propose a view-dependent, ray-tracing transformation scheme called RPT, which efficiently represents high resolution 3D information relating to a view and can be easily decomposed into distributed learning.
3. We leverage the synthetic-view-assisted reconstructions for better inter-phase DVF estimations; this enable us to then optimize 4D CBCT without synthetic data and achieve more reliable performance.
4. We evaluate REGAS on a large scale and realistically simulated CBCT acquisition data. Our experiments show that REGAS reliably reconstructs 4D CBCT from a single 3D CBCT acquisition and significantly outperforms comparable methods.

Related Work

Traditional 4D CBCT Reconstruction

In its fundamental form, 4D CBCT reconstruction is based on the FDK algorithm (Feldkamp, Davis, and Kress 1984). Under the respiratory-gated model, various methods have been proposed to improve 4D CBCT reconstruction. The algebraic approach attempts to improve reconstructions iteratively based on different aspects of image quality and can be generally described as:

$$\hat{V} = \arg \min_V \|AV - P\|^2 + R(V), \quad (1)$$

where V is the reconstructed phase, A is the the projection matrix that describes the voxel-pixel correspondence between V and views P , and $R(V)$ is a regularization term, e.g., total variation (TV). The family of Algebraic Reconstruction Rechniques (ART) (Blondiaux et al. 2017), such as SART and OSSART, falls under this category. Prior Image Constraint Compressive Sensing (PICCS) (Chen 2008) seeks to minimize the total variation and pixel-wise difference between reconstructed phase and a prior image, which can be a prior scan or the reconstruction from using all the observed views. (Ritschl et al. 2012) propose to enforce total variation along the temporal axis. (Mory et al. 2014) propose ROOSTER, which uses various regularizations to reduce noise within a selected region of interest.

DVF-based approaches seek to use the deformation fields between phases to improve reconstructions; however, additional information is often required to find such DVFs. (Brock, Docef, and Murphy 2010; Ren et al. 2012) rely on a previously obtained high-quality 4D CT scan to compute the initial DVFs, and correct them with the currently observed views; the final DVFs are then used to deform the prior high-quality 4D scan to represent patient’s current state. Combinations of algebraic and DVF-based approaches also exist, with algorithms such as SMEIR (Wang and Gu 2013) and MC-SART (Chee et al. 2019). These methods obtain the initial phase reconstructions from an algebraic approach, estimate DVF based on those reconstructions, and iteratively improve both the reconstructions and the DVFs. As initial reconstructions are of low quality, there is no guarantee that DVFs and reconstructions converge simultaneously. In particular, MC-SART requires additional devices to measure diaphragm amplitude and velocity.

Deep Learning-based CT Reconstruction

Deep learning-based methods have obtained impressive results on reconstructing sparse-view CT images (Chen et al. 2020; Han and Ye 2018; Zhang, Li, and Chen 2021). However, these methods are often designed for 2D slice reconstruction, where the computational complexity is reasonable. These methods also rely on supervised training and high quality groundtruth, which limit their application in 4D CBCT as the breathing motion is continuous and does not have an easily measurable groundtruth. 4D-AirNet (Chen et al. 2020), for example, performs their experiments on 2D CT slices despite motivated by 4D CBCT, as the computational cost is otherwise infeasible.

Respiratory-Gated Synthesis (REGAS)

Let $P^{\text{obs}} = \{P^{\text{obs}}(a_k)\}_{k=1}^K$ be K views observed from a single CBCT acquisition process where a_k denotes the angle of the k^{th} view. Through respiratory gating, views of P^{obs} can be binned into several phases with $P^{\text{obs}} = \cup_i P_i^{\text{obs}}$, where P_i^{obs} denotes the set of views from phase i . After binning, we can reconstruct a CBCT image for phase i using views from P_i^{obs} . However, since $|P_i^{\text{obs}}| \ll K$, the reconstructed image suffers from aliasing artifacts. At the core of REGAS, we propose to synthesize the unobserved views P_i^{syn} for all i , such that $|P_i^{\text{obs}}| + |P_i^{\text{syn}}| = K$, and thus reconstructing CBCT images using P_i^{syn} and P_i^{obs} results in less aliasing artifact. In the following sections, we describe the two main components of REGAS: *Ray Path Transformation* (RPT), which is a differentiable projection scheme that enables scalable view synthesis under the Cone-Beam geometry, and a *View Synthesis Network* (VSN) that generates high quality P_i^{obs} with self-supervision.

Ray Path Transformation (RPT)

Processing 4D CBCT data with a reasonable resolution limits the possible capacity of CNNs due to computational constraints. One way to mitigate this limitation is to reduce the input size via patch processing. Assuming the emitted rays traverse in Cartesian planes (e.g., in Parallel-Beam or Fan-Beam CT), one can separate the observed volume into slices [Chen et al.], therefore dramatically reduces the input size. However, it is less straightforward to perform such a separation under a Cone-Beam imaging geometry, as rays traverse multiple Cartesian planes. Motivated by the fact that a tomographic view only partially observes the desired volume during CBCT acquisition, we instead seek to reduce computation by including only the observed volume when synthesizing a tomographic view.

To this end, REGAS implements a Ray Path Transformation (RPT) operator \mathcal{T} . Given a view angle a_k , RPT transforms a CBCT volume from a Cartesian-based representation $V \in \mathbb{R}^{X \times Y \times Z}$ to view-based representation $R_{a_k} \in \mathbb{R}^{W \times H \times S}$, such that $P(a_k, w, h) = \sum_{s=1}^S R_{a_k}(w, h, s)$, where S is the marching dimension of each ray, and $P(a_k) \in \mathbb{R}^{W \times H}$ is the tomographic view under angle a_k . Mathematically, the RPT operator \mathcal{T} can be described as:

$$\mathcal{T}(V, a_k) = R_{a_k}, R_{a_k}(w, h, s) = V(\mathbf{l}_{w,h}^{a_k}(s)), \quad (2)$$

where $\mathbf{l}_{w,h}^{a_k}$ denotes the line segment that connects point (w, h) in $P(a_k)$ and the ray source. As such, $R_{a_k}(w, h, s)$ is the minimum representation of V to produce $P(a_k)$, and can be split and recombined over the $w-h$ plane while maintaining integrity to the Cone Beam forward projection geometry, as demonstrated in Fig. 2. This property enables patch training and for REGAS and scales REGAS to synthesize high resolution views. RPT is implemented through CUDA with gradient propagation, and is as fast as other GPU-based forward projection operations.

View Synthesis Network (VSN)

Two factors are essential in synthesizing reliable unobserved views for different phases. Firstly, the synthesized views of

phase i should be geometrically consistent with the observed views of the same phase, especially over the regions with large motion. Secondly, the synthesized views should be realistic and contain little noise in their texture.

To ensure geometric consistency, we first obtain initial phase reconstructions $V_i^{\text{init}} = \mathcal{H}(P_i^{\text{obs}})$, where \mathcal{H} denotes a reconstruction method, e.g., FDK or SART. While V_i^{init} have low imaging quality, they provide geometric templates to synthesize unobserved views. To synthesize views along angle a_k , we use RPT to obtain R_{i,a_k}^{init} to reduce memory footprint.

As shown in Fig. 2, the View Synthesis Network (VSN) consists of two subnets. The first subnet is a 3D CNN \mathcal{G} with a UNet-like architecture that removes artifacts in R_{i,a_k}^{init} . The forward process of \mathcal{G} can be described as:

$$\{R_{1,a_k}^{\text{ref}}, R_{2,a_k}^{\text{ref}}, \dots, R_{N,a_k}^{\text{ref}}\} = \mathcal{G}(R_{i,a_k}^{\text{init}}) + R_{i,a_k}^{\text{init}} \quad (3)$$

$$R_{i,a_k}^{\text{ref}} = R_{1,a_k}^{\text{init}} \oplus R_{2,a_k}^{\text{init}} \oplus \dots \oplus R_{N,a_k}^{\text{init}},$$

where \oplus concatenates R_{i,a_k}^{init} over the channel dimension. The refined volumes R_{i,a_k}^{ref} are constrained through a self-supervised loss, described as

$$\mathcal{L}_{\text{MA}} = \left\| \frac{1}{N} \sum_i R_{i,a_k}^{\text{ref}} - R_{a_k}^{\text{ma}} \right\|_1, R_{a_k}^{\text{ma}} = \mathcal{T}(V^{\text{ma}}, a_k), \quad (4)$$

where $V^{\text{ma}} = \mathcal{H}(P^{\text{obs}})$ is the motion-affected reconstruction using all observed views. While V^{ma} is blurry over moving anatomical regions, it is of high quality over static anatomical regions. Similarly, R_{i,a_k}^{ref} on average should follow this pattern, especially over empty space.

The second subnet is a 2D CNN \mathcal{F} based on RDN (Zhang et al. 2018) that individually processes views from each phase and can be described as:

$$P_i^{\text{syn}}(a_k) = \mathcal{F}(P_i^{\text{ref}}(a_k)) + P_i^{\text{ref}}(a_k), \quad (5)$$

where $P_i^{\text{ref}}(a_k) = \sum_s R_{i,a_k}^{\text{ref}}(a_k)$. Residual learning is used in Eq. (3) and (5) to promote faster convergence.

Note that, for a given phase i , some of the synthesized views have corresponding $P_i^{\text{obs}}(a_k)$ during CBCT acquisition. We thus constraint its corresponding synthesis with an \mathcal{L}_1 :

$$\mathcal{L}_{\text{rec}} = \|P_i^{\text{syn}}(a_k) - P_i^{\text{obs}}(a_k)\|_1. \quad (6)$$

Such a reconstruction loss also prevents Eq. (4) from making individual R_{i,a_k}^{ref} the same as $R_{a_k}^{\text{ma}}$.

For those synthesized views without corresponding observations, an adversarial loss is employed to ensure that the synthesized views are statistically similar to the observed views of the same phase but at slightly rotated angles,

$$\mathcal{L}_{\text{GAN}}^{\mathcal{D}} = \mathbb{E}[\mathcal{D}(P_i^{\text{obs}}(a_k^*)) - 1]^2 + \mathbb{E}[\mathcal{D}(P_i^{\text{syn}}(a_k)) - 0]^2,$$

$$\mathcal{L}_{\text{GAN}}^{\mathcal{G}} = \mathbb{E}[\mathcal{D}(P_i^{\text{syn}}(a_k)) - 1]^2, \quad (7)$$

where $P_i^{\text{obs}}(a_k^*)$ is a view from P_i^{obs} and has the closet view angle a_k^* to a_k .

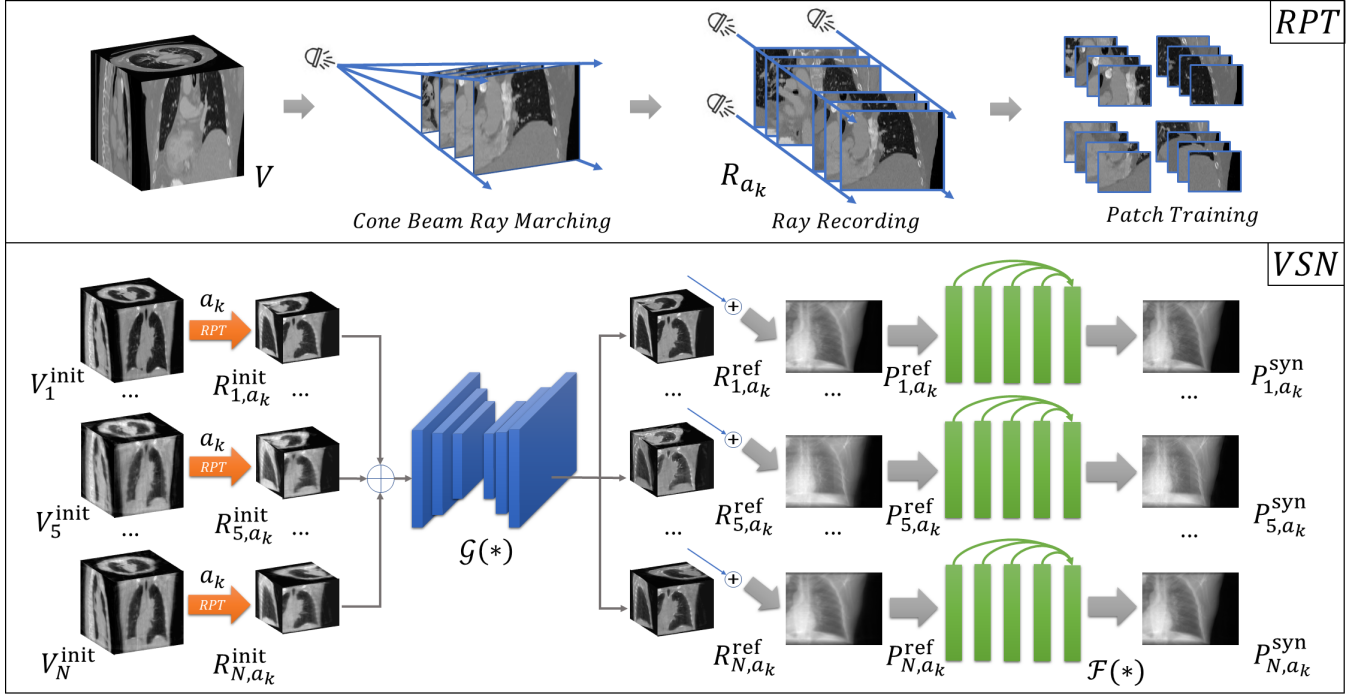


Figure 2: REGAS synthesizes unobserved views for phase i based on observed views across all phases. It first takes the RPT transformed initial reconstructions R_{i,a_k}^{init} and refines them through a 3D network \mathcal{G} . The resulting R_{i,a_k}^{ref} forms views P_{i,a_k}^{ref} and goes through a 2D network \mathcal{F} , yielding P_{i,a_k}^{syn} . After training, P_{i,a_k}^{syn} are used to reconstruct V_i^{syn} . The RPT module generates patch separable volumes with respect to the projection angle, and is differentiable.

The overall loss for training the full REGAS is therefore:

$$\mathcal{L}_{\text{all}} = \lambda_{\text{MA}} \mathcal{L}_{\text{MA}} + \lambda_{\text{rec}} \mathcal{L}_{\text{rec}} + \lambda_{\text{GAN}} \mathcal{L}_{\text{GAN}}, \quad (8)$$

where λ_{MA} , λ_{rec} , and λ_{GAN} are weights for their corresponding losses, and their values are empirically chosen as 1, 0.1, and 0.05, respectively.

Deformation-based Refinement

Combining synthesized and observed views, we can reconstruct phases $V_i^{\text{syn}} = \mathcal{H}(\{P_i^{\text{obs}}, P_i^{\text{syn}}\})$ and obtain images with less severe sparse-view artifacts. However, the detail quality of V_i^{syn} is still lacking due to the imperfect synthetic views. To address this, we apply a deformation-based refinement on V_i^{syn} . Specifically, we estimate the inter-phase Deformation Vector Fields (DVF) $D_{i \rightarrow j}$ through VoxelMorph (Balakrishnan et al. 2019), where i, j indicate the moving and target phases. Based on $D_{i \rightarrow j}$, we perform the following optimization to refine V_i^{syn} :

$$V_i^{\text{out}} = \arg \min_{V_i^{\text{syn}}} \|P_j^{\text{obs}}(a_k) - A(k)D_{i \rightarrow j}V_i^{\text{syn}}\|_2, \forall \{k, j\}, \quad (9)$$

where $A(k)$ is the projection matrix from angle a_k . This step significantly boosts the reconstruction quality as 1. synthetic views are not used in the optimization objective, and 2. the estimated $D_{i \rightarrow j}$ is of high quality due to the lack of artifacts in V_i^{syn} . In fact, we show by experiments that $D_{i \rightarrow j}$ is

close to the upper-bound DVF estimation from groundtruth phases.

In summary, REGAS produces synthetic views to reduce artifacts in V_i^{syn} in a self-supervised manner; It then leverages V_i^{syn} to obtain reliable DVFs such that we can update the reconstructions from only acquired views. As such, REGAS allows the reconstructions to satisfy multi-view consistency from all angles without constraining them to synthetic data. While deformation-based refinement is not restricted to V_i^{syn} and can be applied to V_i^{init} , we find that V_i^{syn} is a much better initialization and leads to better results, as the optimization process in Eq. (9) is non-convex.

Experiments

Dataset. To quantitatively evaluate the effectiveness of respiratory-gated CBCT reconstruction, we follow previous works (Wang and Gu 2013; Chen et al. 2020; Chee et al. 2019) in simulating the acquisition process based on Digitally Reconstructed Radiographs (DRRs) (Milickovic et al. 2000). Specifically, we use the 4D Lung dataset (Hugo et al. 2017), which contains 62 high quality ten-phased 4D Fan-Beam CTs, and the projection geometry from real respiratory-gated acquisitions (Shieh et al. 2019). We set detector size to $\{W = 256, H = 192\}$, detector spacing to 1.55mm , and the total number of acquired views to $K = 680$. CT volumes are normalized to an isotropic resolution of 1.5mm and a resolution of $128 \times 256 \times 256$. While REGAS can be scaled to higher resolutions than $P \in \mathbb{R}^{256 \times 192}$ and

Phase	1	2	3	4	5	6	7	8	9	10	Average
OSSART	37.4/.962	36.8/.956	34.3/.917	36.6/.953	36.8/.956	34.8/.923	34.0/.910	33.0/.889	34.8/.924	34.5/.918	35.3/.931
U-Net	37.4/.966	37.4/.967	35.7/.953	37.3/.967	37.4/.967	36.3/.959	35.4/.951	34.7/.943	36.0/.955	36.0/.956	36.4/.959
DL-PICCS	39.0/.972	38.9/.973	36.9/.959	38.8/.972	39.0/.973	37.5/.965	36.5/.953	35.5/.945	37.0/.956	37.3/.962	37.6/.963
REGAS ^{noDVF}	40.6/.980	40.2/.978	38.8/.970	40.0/.977	40.1/.977	39.1/.974	37.9/.961	36.8/.951	38.5/.966	38.5/.966	39.1/.970
OSSART ^{TTV}	38.3/.975	38.2/.975	37.6/.971	38.0/.974	38.1/.974	37.2/.968	36.7/.962	36.4/.958	36.5/.959	36.2/.954	37.3/.967
SMEIR	39.9/.977	39.6/.977	38.5/.973	40.0/.978	39.7/.977	38.6/.973	37.5/.968	36.0/.958	38.3/.971	38.2/.971	38.6/.972
REGAS	43.6/.989	43.4/.988	42.8/.987	43.6/.989	43.4/.988	42.4/.986	41.8/.984	41.2/.982	42.4/.986	42.1/.985	42.7/.986
DVF-GT	43.8/.987	43.9/.987	43.3/.986	44.1/.988	43.8/.987	42.9/.985	42.5/.984	41.9/.982	43.1/.985	43.0/.985	43.3/.986

Table 1: Quantitative evaluation of 4D CBCT reconstruction on 4D Lung (Hugo et al. 2017) in terms of PSNR and SSIM. The best results are in **bold** besides the reference DVF-GT. Phases that have more observed views have higher PSNRs in their OSSART reconstructions.

$V \in \mathbb{R}^{128 \times 256 \times 256}$, these resolutions are selected to ensure that other comparative methods stay computationally feasible in memory and time. The phase-view correspondences are based on real measurements in (Shieh et al. 2019) after aligning the max-inhale and max-exhale phases with (Hugo et al. 2017). We use OSSART to obtain V_i^{init} . For RPT, the ray marching dimension is set to $S = 128$; during training $R_{i,a,k}^{\text{init}}$ are separated into patches of $128 \times 128 \times 128$. While our REGAS method is self-supervised, thus requiring no training data, the comparative DL-based supervised methods (U-Net and DL-PICCS) are trained on LIDC-IDRI (Armatto III et al. 2011), which contains 890 FBCT lung images after pre-processing. The same data generation method is used to obtain the undersampled reconstructions as inputs, where for each image three random phases and their respective P_i^{obs} are selected.

Implementation Details

The VSN in REGAS is trained end-to-end with an Adam optimizer, which uses a momentum of 0.5 and a learning rate of 0.0001 until convergence. For 3D CNN, REGAS uses a 3D-UNet (Ronneberger, Fischer, and Brox 2015) structure, where five downsampling and upsampling CNN layers are used. A 2D Residual DenseNet (RDN (Zhang et al. 2018)) is used for the view-refining stage, where we use ten residual dense blocks, each of which has six convolution layers and growing rate of thirty-two. We use 10 NVIDIA 2080TI to train the network in one day. While patch training is used due to the memory cost of backpropagation, at inference time P^{syn} are generated with full resolution. It takes 28.75ms to synthesize one view, or 176s to synthesize all views for one 4D CBCT image on a single NVIDIA 2080TI. We use VoxelMorph (Balakrishnan et al. 2019) for DVF estimation, where all V_i^{syn} are used for training. We use 6 NVIDIA 2080TI GPUs to train VoxelMorph for one day to obtain the desired model. This is similarly done for all methods that use inter-phase modelling, i.e. SMEIR^{sim} and DVF-GT. We use TIGRE¹ for OSSART reconstruction. Please see the supplemental material section for more details.

¹<https://github.com/CERN/TIGRE>

Quantitative Evaluations

We summarize the quantitative comparisons of different reconstruction approaches against REGAS in Table 1. These approaches include:

- OSSART (Andersen and Kak 1984): A classic algebraic sparse-view reconstruction method; spatial TV is used to ensure smoothness in reconstructed images.
- OSSART^{TTV}: OSSART with an additional Temporal TV term during reconstruction optimization, similar to (Ritschl et al. 2012).
- U-Net: A supervised DL method based on the 3D U-Net architecture, representative of end-to-end approaches like (Han and Ye 2018).
- DL-PICCS (Zhang, Li, and Chen 2021): A multi-staged supervised DL method that applies PICCS between stages.
- SMEIR^{sim}: A DVF-based optimization method based on (Wang and Gu 2013), where the DVFs are estimated from OSSART reconstructions.
- DVF-GT: An upper-bound analysis on the DVF-based refinement approach, where the DVFs are obtained from groundtruth images.

We visualize the results in Fig. 3 over different phases. As we can see for OSSART, due to motion-induced irregular sampling, aliasing artifacts vary in phases 1 and 8, which have 105 and 50 P_i^{obs} respectively. Details like rib bones are difficult to distinguish in phase 8, and clearer in phase 1. For clarity, we divide the rest of the baselines based on whether they model inter-phase information or not.

Single-phase-only modelling approaches. Here we mainly focus on DL-based methods, as they are the current state of the art in sparse-view CT reconstruction without inter-phase modelling. The U-Net approach, which operates purely in the image space, clearly suffers from over-smoothing, especially in phase 8, as the pixel-wise loss leads to averaging when artifact is severe. This is somewhat improved in DL-PICCS, which contains two U-Nets. The results from the first U-Net are updated with P_i^{obs} in an OSSART manner, which recovers some lost details that can be observed in OSSART. Despite such an update, the bone details are still not fully recovered in phase 8.

Phase	OSSART	U-Net	DL-PICCS	REGAS ^{noDVF}	OSSART ^{TTV}	SMEIR	REGAS	DVF-GT	GT
1									
	36.68/0.958	36.98/0.964	38.48/0.971	<u>39.80/0.976</u>	37.43/0.971	38.48/0.972	42.38/0.986	42.12/0.984	PSNR/SSIM
5									
	36.12/0.952	36.75/0.963	38.42/0.971	<u>39.08/0.973</u>	37.22/0.970	38.70/0.974	42.27/0.986	42.74/0.985	PSNR/SSIM
8									
	32.42/0.880	34.20/0.939	35.13/0.941	<u>36.13/0.947</u>	35.56/0.953	35.28/0.953	40.55/0.980	40.57/0.977	PSNR/SSIM

Figure 3: Visual comparisons of 4D reconstructions by different methods for phases 1 and 8. The best generation metrics are bold, the second best is underlined. Metrics are calculated volume-wise, and the difference maps are provided below the reconstruction images.

We note that there are DL-based methods that attempt to leverage the temporal information, such as 4D-AirNet (Chen et al. 2020). However, 4D-AirNet is constrained to work on 2D slices instead of the native 3D space for Cone Beam geometry, as the GPU memory cost would be infeasible if the network is updated with 3D kernels. As such, it is restricted to Fan Beam geometry if view consistency is to be enforced.

While DL-PICCS is chosen as a representative baseline, as it has a step to ensure view consistency like 4D-AirNet and is trained in two stages to avoid memory constraints; we note that DL-PICCS uses all memory in a NVIDIA 2080Ti GPU with a batch size of one. Compute feasibility is an important factor in DL-based methods, and is a strength of REGAS. REGAS addresses the undersampling problem by synthesizing views instead of directly operating in the higher-dimension image space. With RPT, REGAS can be trained in patches while preserving CBCT geometry; this greatly scales its ability to use deeper networks while still generating high quality views. While RPT is used for reconstruction in REGAS, its functions to obtain minimum 3D repre-

sentation with respect to a view and to propagate gradients are generally useful, such as for any DL-based method that looks to leverage CT and X-ray images together for learning. Finally, REGAS is self-supervised, and can avoid domain gaps such as scanner or patient differences from a training set. While P_i^{syn} are not perfect and still lead to some artifacts, as in Fig. 3 for REGAS^{noDVF}, bone details are much better recovered.

Inter-phase modelling approaches. Here, the dominant approaches are non-DL-based approaches, which are less reliant on GPU memory and leverage the temporal correlations between phases. A common approach is to add a Temporal TV term during the reconstruction optimization process, as represented by OSSART^{TTV}. While OSSART^{TTV} greatly out-performs OSSART in PSNR, its superior performance is based on the fact that the phase voxels are mostly stationary with each other; however, details remain blurry due to movements, as such errors around the edges are very high.

SMEIR focuses on finding the optimal DVFs between phases from limited acquisition, such that we can recon-

struct phases with P^{obs} as described in Eq. (9). Specifically, it finds DVFs through an iterative scheme, where (i) DVFs are first estimated from initial SART reconstructions, (ii) a reference phase is updated following Eq. (9), and (iii) DVFs are updated based on observed views from other phases and the reference phase. Steps 2 and 3 are repeated to obtain better reference phase and DVFs. SMEIR contains many hyper-parameters for its iterative optimization process, and does not have a public implementation for reference. Furthermore, as stated by the authors, the DVFs are not guaranteed to converge. To avoid an unfaithful re-implementation, we simplify SMEIR to steps 1 and 2 with no iteration, referred to as SMEIR^{sim}. SMEIR^{sim} is comparable to REGAS since both involve a reconstruction step and a DVF-based refinement step. Similarly, both should benefit from iterative updates if they converge. We observe that due to the superior reconstructions of REGAS from synthesized views, the DVFs are estimated with more accuracy and lead to high quality reconstructions. The artifacts from REGAS^{noDVF} are gone, as only real acquisitions are used. In comparison, while the SMEIR^{sim} results are seemingly alias-free, the erroneous DVFs lead to inconsistent deformations around the body surface, which can be observed in the phase 8 difference image in Fig. 3.

Upper-bound analysis. We also perform an upper-bound analysis called DVF-GT, where the DVFs are estimated directly from groundtruth phases and used in Eq. (9). Since there does not exist a perfect DVF that leads to lossless phase reconstruction, DVF-GT represents the upper bounds of the DVF-based refinement step. We find that REGAS approaches DVF-GT in performance, particularly in SSIM where REGAS is on par with DVF-GT. As such, we believe that REGAS approaches the upper limit from DVF-based refinement.

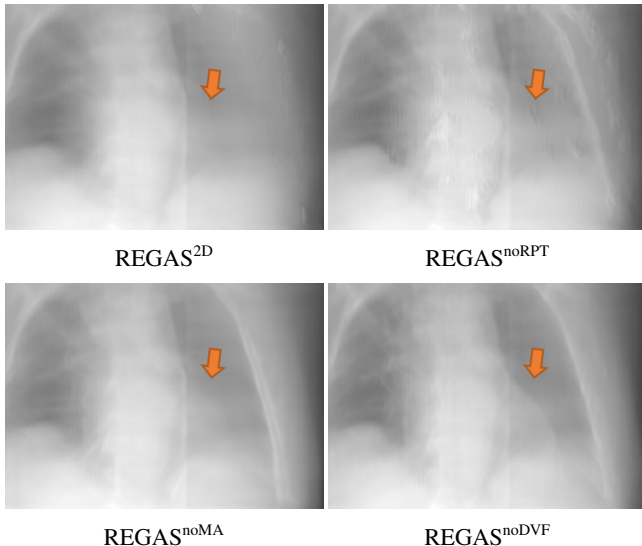


Figure 4: Visual Comparison of synthesized projections over various ablated methods, taken from phase 7.

Ablation study. We examine the effective of individual

Method	\mathcal{G}	RPT	\mathcal{L}_{MA}	Avg. Perf.
REGAS ^{2D}	✗	✗	✗	36.09/0.938
REGAS ^{noRPT}	✓	✗	✓	36.49/0.946
REGAS ^{noMA}	✓	✓	✗	37.96/0.964
REGAS ^{noDVF}	✓	✓	✓	39.05/0.970

Table 2: Ablation comparison among different implementations of REGAS. The average performance across all phases is presented.

components in REGAS. REGAS^{2D} trains the 2D CNN \mathcal{F} with \mathcal{L}_{rec} and \mathcal{L}_{GAN} by directly using projections from V_i^{init} . With a 3D CNN \mathcal{G} , REGAS^{noRPT} does not use RPT and has to downsample V_i^{init} to $\mathbb{R}^{128 \times 128 \times 128}$ to be memory-wise viable. REGAS^{noMA} does not use \mathcal{L}_{MA} , which denoises in 3D. As we can see in Table 2, adding \mathcal{G} , RPT, and \mathcal{L}_{MA} each has a positive effect on performance. We show an instance of the synthesized views in Fig. 4 for all versions of REGAS. In particular, we can see that views from REGAS^{noRPT} and REGAS^{noMA} both recover the rib cage frame on the right side of the lung. Compared to the full REGAS, there is less clarity over the heart region in REGAS^{noMA} due to the noisier 3D CTs, and REGAS^{noRPT} generates more fictitious details. The full REGAS produces a much more stable and geometrically consistent synthesis by leveraging DVF estimations from REGAS^{noRPT} and real observations, which do not contain synthetic details. As such, we demonstrate the utility of each component and the effectiveness of scaling computation complexity with distributed forward projections. Please refer to the supplemental material on how volumetric resolution impacts views visually and other intermediate results.

Conclusion

We propose REGAS, a novel 4D CBCT reconstruction method from a single 3D CBCT acquisition. On a high level, REGAS first formulates sparse-view phase reconstruction as a synthesis problem on unobserved views. By combining observed and synthesized views, REGAS can obtain reconstructions with significantly less artifacts. REGAS then finds inter-phase DVFs based on these reconstructions, and use a synthesis-free optimization to refine reconstructions based on DVFs and observed views. Within REGAS, we propose RPT, which transforms a CT volume into a ray-based representation. The RPT-transformed volumes can be separated for distributed, patch-based training without affecting the Cone Beam imaging geometry, which addresses the memory bottleneck during network training. REGAS' network is trained in a self-supervised manner and does not require groundtruth on unobserved views, and is practical for clinical application. Our evaluation on a 4D Lung dataset show that REGAS significantly outperforms comparable methods in reconstruction performance. REGAS can assist in more accurate CBCT-based image-guided radiation therapy with high quality reconstructions. Since RPT reduces the memory footprint of 3D volume in a DL-based 3D-to-2D hybrid system, it can be applied to tasks that benefit from fusion learning on 3D CT and 2D radiographs, e.g. landmark detection, lesion segmentation, without sacrificing resolution.

References

- Andersen, A. H.; and Kak, A. C. 1984. Simultaneous algebraic reconstruction technique (SART): a superior implementation of the ART algorithm. *Ultrasonic imaging*, 6(1): 81–94.
- Armato III, S. G.; McLennan, G.; Bidaut, L.; McNitt-Gray, M. F.; ; et al. 2011. The lung image database consortium (LIDC) and image database resource initiative (IDRI): a completed reference database of lung nodules on CT scans. *Medical physics*, 38(2): 915–931.
- Balakrishnan, G.; Zhao, A.; Sabuncu, M. R.; Guttag, J. V.; and Dalca, A. V. 2019. VoxelMorph: A Learning Framework for Deformable Medical Image Registration. *IEEE Trans. Medical Imaging*, 38(8): 1788–1800.
- Beaudry, J. 2015. *4D cone-beam CT image reconstruction of Varian TrueBeam v1.6 projection images for clinical quality assurance of stereotactic ablative radiotherapy to the lung*. Ph.D. thesis, University of British Columbia.
- Blondiaux, E.; Cochet, A.; Durand, E.; Kremer, S.; Montaudon, M.; Parlier-Cuau, C.; et al. 2017. *Imagerie médicale: les fondamentaux: radioanatomie, biophysique, techniques et sémiologie en radiologie et médecine nucléaire*. Elsevier Health Sciences.
- Brock, R. S.; Docef, A.; and Murphy, M. J. 2010. Reconstruction of a cone-beam CT image via forward iterative projection matching. *Medical physics*, 37(12): 6212–6220.
- Chee, G.; O’Connell, D.; Yang, Y.; Singhrao, K.; Low, D.; and Lewis, J. 2019. McSART: an iterative model-based, motion-compensated SART algorithm for CBCT reconstruction. *Physics in Medicine & Biology*, 64(9): 095013.
- Chen, G.; Zhao, Y.; Huang, Q.; and Gao, H. 2020. 4D-AirNet: a temporally-resolved CBCT slice reconstruction method synergizing analytical and iterative method with deep learning. *Phys Med Biol*, 65(17): 175020.
- Chen, G. H. 2008. A Method to Accurately Reconstruct Dynamic CT Images from Highly Undersampled Projection Data Sets. *Med. Phys.*, Feb, 35(2): 660–663.
- Elstrøm, U. V.; Muren, L. P.; Petersen, J. B. B.; and Grau, C. 2011. Evaluation of image quality for different kV cone-beam CT acquisition and reconstruction methods in the head and neck region. *Acta Oncologica*, 50(6): 908–917.
- Feldkamp, L. A.; Davis, L. C.; and Kress, J. W. 1984. Practical cone-beam algorithm. *J. Opt. Soc. Am. A*, 1(6): 612–619.
- Han, Y.; and Ye, J. C. 2018. Framing U-Net via Deep Convolutional Framelets: Application to Sparse-View CT. *IEEE Trans. Medical Imaging*, 37(6): 1418–1429.
- Hugo, G. D.; Weiss, E.; Sleeman, W. C.; Balik, S.; Keall, P. J.; Lu, J.; and Williamson, J. F. 2017. A longitudinal four-dimensional computed tomography and cone beam computed tomography dataset for image-guided radiation therapy research in lung cancer. *Medical Physics*, 44(2).
- Milickovic, N.; Baltas, D.; Giannouli, S.; Lahanas, M.; and Zamboglou, N. 2000. CT imaging based digitally reconstructed radiographs and their application in brachytherapy. *Physics in Medicine & Biology*, 45(10): 2787.
- Mory, C.; Auvray, V.; Zhang, B.; Grass, M.; Schäfer, D.; Chen, S. J.; Carroll, J. D.; Rit, S.; Peyrin, F.; Douek, P.; et al. 2014. Cardiac C-arm computed tomography using a 3D+ time ROI reconstruction method with spatial and temporal regularization. *Medical physics*, 41(2): 021903.
- Ren, L.; Chetty, I. J.; Zhang, J.; Jin, J.-Y.; and et al. 2012. Development and clinical evaluation of a three-dimensional cone-beam computed tomography estimation method using a deformation field map. *International Journal of Radiation Oncology* Biology* Physics*, 82(5): 1584–1593.
- Ritschl, L.; Sawall, S.; Knaup, M.; Hess, A.; and Kachelrieß, M. 2012. Iterative 4D cardiac micro-CT image reconstruction using an adaptive spatio-temporal sparsity prior. *Physics in Medicine and Biology*, 57(6): 1517–1525.
- Ronneberger, O.; Fischer, P.; and Brox, T. 2015. U-Net: Convolutional Networks for Biomedical Image Segmentation. In *Medical Image Computing and Computer-Assisted Intervention - MICCAI*, volume 9351 of *Lecture Notes in Computer Science*, 234–241. Springer.
- Shieh, C.-C.; Gonzalez, Y.; Li, B.; Jia, X.; Rit, S.; Mory, C.; Riblett, M.; Hugo, G.; Zhang, Y.; Jiang, Z.; et al. 2019. SPARE: Sparse-view reconstruction challenge for 4D cone-beam CT from a 1-min scan. *Medical physics*, 46(9): 3799–3811.
- Wang, J.; and Gu, X. 2013. Simultaneous motion estimation and image reconstruction (SMEIR) for 4D cone-beam CT. *Medical physics*, 40(10): 101912.
- Yan, H.; Wang, X.; Yin, W.; Pan, T.; Ahmad, M.; Mou, X.; Cerviño, L.; Jia, X.; and Jiang, S. B. 2013. Extracting respiratory signals from thoracic cone beam CT projections. *Physics in Medicine & Biology*, 58(5): 1447.
- Zhang, C.; Li, Y.; and Chen, G.-H. 2021. Accurate and robust sparse-view angle CT image reconstruction using deep learning and prior image constrained compressed sensing (DL-PICCS). *Medical Physics*, 48(10): 5765–5781.
- Zhang, Y.; Tian, Y.; Kong, Y.; Zhong, B.; and Fu, Y. 2018. Residual Dense Network for Image Super-Resolution. In *2018 IEEE CVPR 2018, Salt Lake City, UT, USA, June 18-22, 2018*, 2472–2481.